


Article

Measurement of CeO₂ Nanoparticles in Natural Waters Using a High Sensitivity, Single Particle ICP-MS

Ibrahim Jreije¹, Agil Azimzada^{1,2}, Madjid Hadioui¹ and Kevin J. Wilkinson^{1,*} 

¹ Biophysical Environmental Chemistry Group, University of Montreal, P.O. Box 6128, Succ. Centre-Ville, Montreal, QC H3C 3J7, Canada; ibrahim.jreije@umontreal.ca (I.J.); agil.azimzada@mail.mcgill.ca (A.A.); Madjid.hadioui@umontreal.ca (M.H.)

² Department of Chemical Engineering, McGill University, Montreal, QC H3C 3J7, Canada

* Correspondence: kj.wilkinson@umontreal.ca; Tel.: +1-514-343-6741

Academic Editor: Zikri Arslan

Received: 2 November 2020; Accepted: 23 November 2020; Published: 25 November 2020



Abstract: As the production and use of cerium oxide nanoparticles (CeO₂ NPs) increases, so does the concern of the scientific community over their release into the environment. Single particle inductively coupled plasma mass spectrometry is emerging as one of the best techniques for NP detection and quantification; however, it is often limited by high size detection limits (SDL). To that end, a high sensitivity sector field ICP-MS (SF-ICP-MS) with microsecond dwell times (50 μs) was used to lower the SDL of CeO₂ NPs to below 4.0 nm. Ag and Au NPs were also analyzed for reference. SF-ICP-MS was then used to detect CeO₂ NPs in a Montreal rainwater at a concentration of $(2.2 \pm 0.1) \times 10^8 \text{ L}^{-1}$ with a mean diameter of $10.8 \pm 0.2 \text{ nm}$; and in a St. Lawrence River water at a concentration of $((1.6 \pm 0.3) \times 10^9 \text{ L}^{-1})$ with a higher mean diameter ($21.9 \pm 0.8 \text{ nm}$). SF-ICP-MS and single particle time of flight ICP-MS on Ce and La indicated that 36% of the Ce-containing NPs detected in Montreal rainwater were engineered Ce NPs.

Keywords: nanoparticles; cerium oxide; single particle ICP-MS; sector field; time of flight; natural waters

1. Introduction

Due to their unique properties, engineered nanomaterials are now widely used in numerous commercial products. Cerium oxide (CeO₂) nanoparticles (NPs) are among the most commonly used engineered NPs, with applications in catalysis [1–3], the manufacturing of semiconductors [2], biomedicine [4] and agriculture [5], among other fields. For example, they are commonly found as UV filters in sunscreens, additives in diesel fuels and as a component of paints and stains [6,7]. With the significant increase in the production and use of CeO₂ NPs, concern is increasing over their release into the environment and their subsequent fate and toxicity. Among their important environmental pathways, CeO₂ NPs can be released into the air by diesel emissions; into soils from solid waste and recycling and into aquatic systems from the effluents of wastewater treatment plants [1]. Furthermore, a number of recent papers [8–10] have measured the release of CeO₂ NP from surface coatings such as paints and stains. Nonetheless, the vast majority of data on the concentrations, fate and transformations of CeO₂ NP in the environment have been generated by modelling [11,12], or extrapolated from release studies performed under controlled laboratory conditions. This is mainly because the direct analysis of CeO₂ NPs in the environment is extremely challenging due to their small sizes (often below 20 nm), their low concentrations (on the order of ng L⁻¹) and the complexity of environmental matrices, which also contain natural colloids.

Techniques based upon inductively coupled plasma mass spectrometry (ICP-MS) are likely to be the most promising for detecting and quantifying inorganic NP in biological and environmental samples. Particle size distributions can be obtained either by coupling a separation technique such as field flow fractionation (FFF) [13] or hydrodynamic chromatography (HDC) [14] upstream of the ICP-MS or by performing ultrafast measurements on single particles (single particle (SP) ICP-MS). SP-ICP-MS combines the specificity and sensitivity of mass spectrometry with a particle-by-particle analysis, enabling quantification of very low NP concentrations (ng L^{-1}) and information on their number concentrations, sizes, and size distributions. Transient ion clouds that are created from the NP in the plasma (typically 300–500 μs) are directly related to the particle number concentrations, while the signal intensity is related to particle (elemental) mass [15]. For a given NP composition, density and geometry, particle size can be calculated.

The very small NPs are expected to have a greater environmental risk, due to their increased propensity to cross biological membranes [16,17]. Therefore, it is especially important to obtain rigorous size, concentration, and fate data for the smallest NP. The minimal particle size (size detection limit = SDL) that can be measured by SP-ICP-MS depends largely upon the signal to noise ratio. A number of approaches have been employed to decrease the SDL [18] including: sample dilution, judicious choice of isotopes, interference removal strategies [19,20], shorter dwell times [21], etc.

The first objective of this study was to decrease the SDL for CeO_2 NPs using a high sensitivity sector field ICP-MS (SF-ICP-MS), very short dwell times (<100 μs) and the introduction of a dry aerosol. The optimized method was then used to detect, quantify, and characterize CeO_2 NPs in several natural water samples.

2. Results and Discussion

2.1. Optimization of SP-ICP-MS for CeO_2 NPs

In single particle ICP-MS, size detection limits (SDL) are minimized for Ce NPs by optimizing the signal/noise (S/N) for $^{140}\text{Ce}^+$. In this case, noise includes both electronic noise and background concentrations, comprised of isobaric and polyatomic interferences, dissolved Ce and Ce NPs that are smaller than the SDL. The impact of dwell times on the SDL [21] was first tested on a suspension of CeO_2 NPs in Milli-Q water, with or without dissolved Ce. While both spike intensity and background signal decreased as dwell time was decreased from 500 to 20 μs (Figure S1), S/N was clearly improved at the shorter dwell times (Figure 1). For example, for a decrease in dwell time from 500 μs to 20 μs , the SDL decreased from 4 nm to 2.2 nm in Milli-Q water (Figure 1A) and from 6.2 nm to 3.8 nm when the data were acquired in the presence of 10 ng L^{-1} of dissolved Ce (Figure 1B). Although the lowest SDL was measured with a 20 μs dwell time, it was not used further here since analysis was limited to one million datapoints per run (and thus an overall analysis time of 20 s). For environmental samples, longer acquisition times better ensure representativity by better taking into account sample polydispersity and low particle numbers. Given the slight difference in SDL between dwell times of 20 and 50 μs (Figure 1), a dwell time of 50 μs and a corresponding 50 s acquisition time were used in a majority of subsequent experiments.

Sensitivity and transport efficiency were determined for gold, silver and CeO_2 NPs using a quadrupole based ICP-MS (Q-ICP-MS) and a SF-ICP-MS, using wet or dry (i.e., desolvator) sample introduction. Sensitivity increased about 100 \times for Ag and 200 \times for Au and Ce when using the SF-ICP-MS as compared to the Q-ICP-MS (Table 1). This increase of sensitivity led to a lowering of the SDL from 16.3 to 4.7 nm for Ag; from 19.0 to 4.4 nm for Au and from 16.8 to 4.0 nm for CeO_2 . For the Q-ICP-MS, similar SDL have previously been reported for CeO_2 in the literature [7,22]. When the sample was introduced as a dry aerosol, sensitivity increased a further 5 \times for Ag and Au and 3 \times for Ce, resulting in a lowering of the SDLs to 3.1 nm (Ag), 2.8 nm (Au) and 2.3 nm (CeO_2) (Table 1).

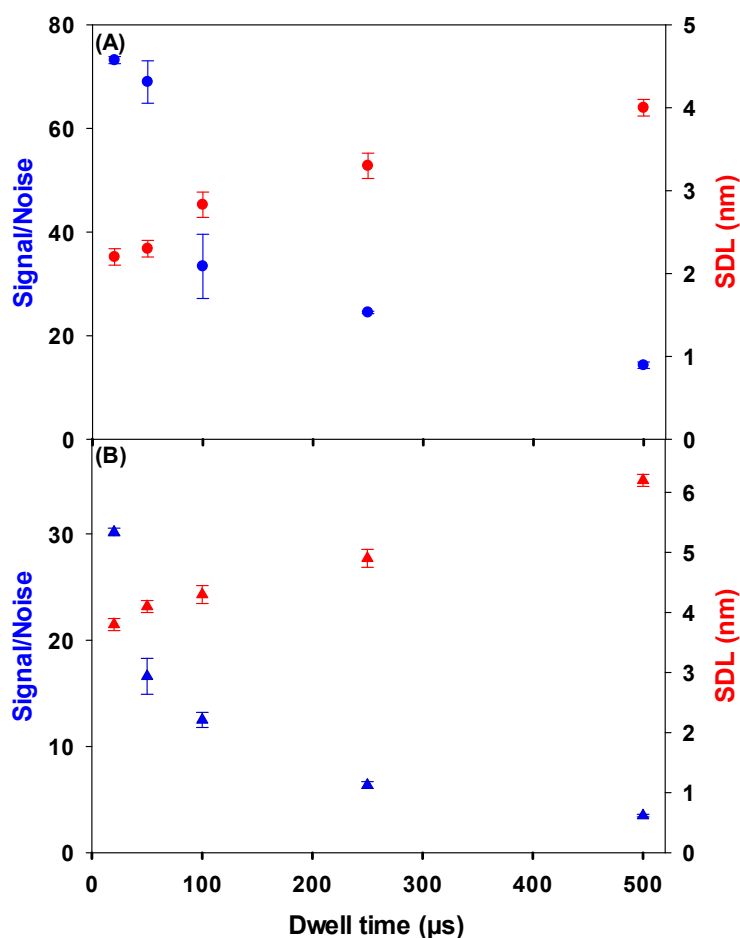


Figure 1. Signal: Noise (blue) and size detection limits (red) as a function of dwell time for: (A) a 10 ng L^{-1} suspension of CeO_2 NPs (1–10 nm) in Milli-Q water; (B) a 10 ng L^{-1} suspension of CeO_2 NPs (1–10 nm) in a Milli-Q water containing 10 ng L^{-1} of ionic Ce. Signal/Noise was determined by dividing the average intensity of a well resolved peak of a 9 nm CeO_2 NP by the average intensity of the continuous background. All measurements were obtained using SF-ICP-MS and sample introduction via a desolvator.

Table 1. Sensitivity for Ag, Au and Ce and the resulting size detection limits for Ag, Au and CeO_2 NPs in Milli-Q water obtained using a quadrupole (Q-) or sector field (SF-) ICP-MS running with (dry) or without a desolvator (wet). A $50 \mu\text{s}$ dwell time was used. Means and standard deviations are obtained from analysis on three different dates.

Analyte	Sensitivity (Counts fg^{-1})			Nanoparticle	Size Detection Limit (nm)		
	Q-ICP-MS	SF-ICP-MS			Q-ICP-MS	SF-ICP-MS	
		Wet	Dry			Wet	Dry
Ag	50 ± 19	4750 ± 1200	$22,300 \pm 2400$	Ag	16.3 ± 2.1	4.7 ± 0.2	3.1 ± 0.3
Au	15 ± 3	2900 ± 800	$13,700 \pm 1200$	Au	19.0 ± 1.0	4.4 ± 0.1	2.8 ± 0.1
Ce	72 ± 15	$14,800 \pm 700$	$47,900 \pm 8600$	CeO_2	16.8 ± 1.1	4.0 ± 0.2	2.3 ± 0.2

The role of membrane desolvation was further evaluated by comparing size distributions and particle number concentrations for small Ag, Au and CeO_2 NPs (nominally 10 nm Ag, 10 nm Au and 1–10 nm CeO_2), using both dry and wet aerosol introduction (Table 2). Some smaller NPs were detected using the dry-SP-ICP-MS due to the lower SDL, consequently leading to higher particle number concentrations (approximately $1.5\times$ more NPs when compared to wet aerosol injection) and a lower average particle size (Figure 2).

Table 2. Average particle sizes, number concentrations and SDL in 10 ng L⁻¹ suspensions of Ag, Au and CeO₂ NPs. Means and standard deviations are obtained from the analysis of triplicate samples.

NP Suspension	Average Particle Size (nm)		NP Number Concentration (×10 ⁷ L ⁻¹)		SDL (nm)	
	Wet	Dry	Wet	Dry	Wet	Dry
Ag	9.3 ± 0.4	8.5 ± 0.1	5.5 ± 0.6	7.7 ± 0.2	4.6 ± 0.1	3.1 ± 0.1
Au	11.8 ± 0.1	9.7 ± 0.1	6.6 ± 0.8	8.9 ± 0.1	4.2 ± 0.1	3.1 ± 0.1
CeO ₂	8.0 ± 0.1	6.3 ± 0.0	20.9 ± 0.4	26.3 ± 1.5	4.1 ± 0.1	2.8 ± 0.1

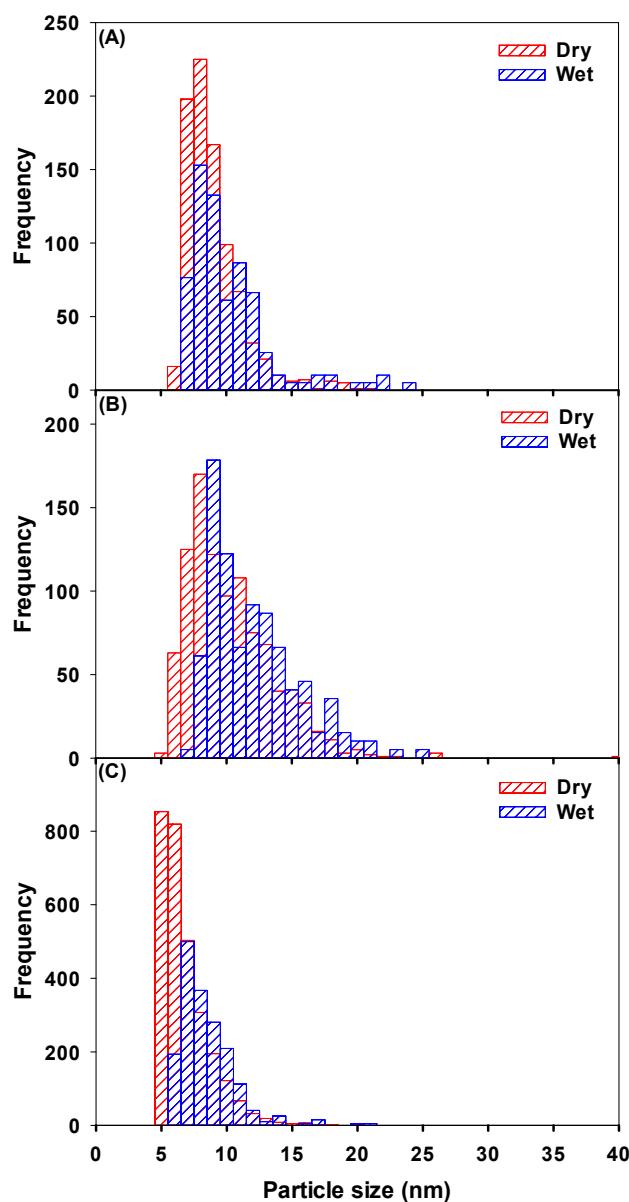


Figure 2. Particle size distributions as measured by wet-SF-ICP-MS (blue) and dry-SF-ICP-MS (red) for 3 suspensions of a small NP: (A) Ag: the mean particle size ± polydispersity of the suspension was 8.5 ± 2.2 with dry introduction and 9.8 ± 3.3 with wet introduction; (B) Au: the mean particle size ± polydispersity of the suspension was 9.8 ± 3.4 with dry introduction and 11.8 ± 3.6 with wet introduction; (C) CeO₂: the mean particle size ± polydispersity of the distribution in the suspension was 6.3 ± 2.0 with dry introduction and 8.0 ± 2.1 with wet introduction.

The difference between the two setups became more significant for an increasing proportion of dissolved metal in the suspensions, which reversed the impact of the desolvator. For example, when a 10 ng L^{-1} suspension of CeO_2 NPs was spiked with 10 ng L^{-1} of dissolved Ce, particle size distributions were similar, with similar average sizes ($8.1 \pm 0.1 \text{ nm}$ for dry-SF-ICP-MS and $8.3 \pm 0.1 \text{ nm}$ for wet-SF-ICP-MS) (Figure S2A), however, nearly $1.6\times$ more CeO_2 NPs were detected using wet-SF-ICP-MS as compared to dry-SF-ICP-MS. Moreover, when a 10 ng L^{-1} suspension of CeO_2 NPs was spiked with 50 ng L^{-1} of dissolved Ce, significantly different particle number concentrations were measured with the two introduction systems with nearly $5\times$ more CeO_2 NPs detected by wet-SF-ICP-MS (Figure S2B). It would appear that when using the desolvator, both the background signal and the NP signal increased, however, background increased to a greater proportion. Therefore, in the presence of significant dissolved metal, the S/N decreased when using dry-SF-ICP-MS as compared to the wet-SF-ICP-MS (Figure S3). For example, for a 9.0 nm CeO_2 NP combined with 50 ng L^{-1} of dissolved Ce, the S/N was 2.8 ± 0.3 when using dry-SF-ICP-MS and 6.8 ± 0.1 when using wet-SF-ICP-MS. When NP suspensions containing increasing dissolved Ce were analyzed in single particle SF-ICP-MS, results clearly showed that the desolvator was more sensitive to the presence of the dissolved fraction with higher SDLs as compared to the wet-SF-ICP-MS (Figure S4). Therefore, although smaller SDLs could be determined by dry-SF-ICP-MS for very low concentrations of dissolved Ce; due to an unknown and variable proportion of dissolved Ce, the introduction of a wet aerosol was prioritized for natural samples.

2.2. Ce-Containing NPs in Natural Waters: Rainwater

The wet-SF-ICP-MS was first used to determine whether Ce NP could be detected in rain. In the rainwater matrix alone, significant numbers of Ce-containing NPs were found, with a mean particle diameter of $10.8 \pm 0.2 \text{ nm}$ (Figure 3C, calculated under the assumption that the particles were spherical CeO_2 NPs). Subsequently, 10 ng L^{-1} of $1\text{--}10 \text{ nm}$ CeO_2 NPs were spiked into the rainwater and compared with observations performed in Milli-Q water. An average particle diameter of $7.9 \pm 0.2 \text{ nm}$ was determined in Milli-Q water (Figure 3A), which was smaller than the size obtained for the NP spiked into rainwater ($9.5 \pm 0.4 \text{ nm}$, Figure 3B). About three times more CeO_2 NPs were detected in the spiked rainwater ($5.1 \times 10^8 \text{ NPs L}^{-1}$) as compared to the spiked Milli-Q water ($1.6 \times 10^8 \text{ NPs L}^{-1}$), which was reasonable given the initial NP numbers found in the unspiked rainwater ($3.8 \times 10^8 \text{ NPs L}^{-1}$). These values corresponded to a recovery for the spike of $84 \pm 16\%$. The slightly smaller than expected recovery could be attributed to an increased aggregation of CeO_2 NPs in the natural precipitation (increased ionic strength), as compared to the Milli-Q water. Note that recovery of total Ce in the rainwater, determined on acidified samples, was $78 \pm 24\%$.

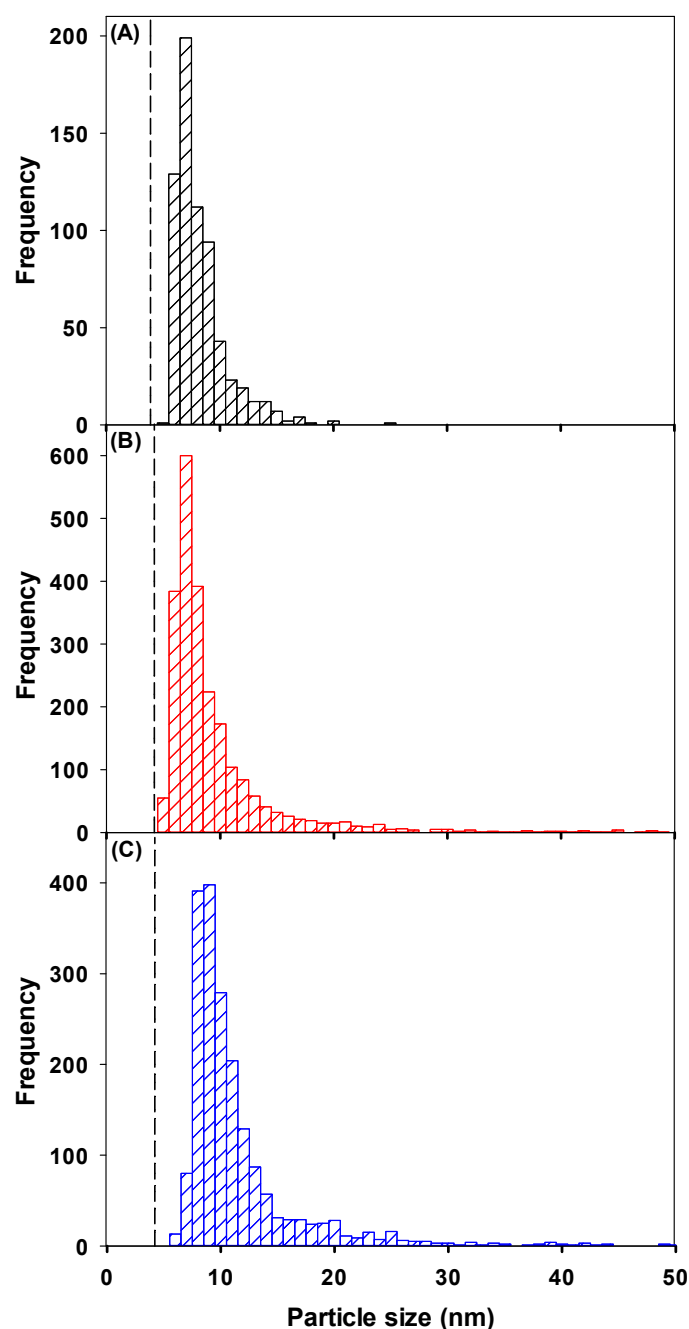


Figure 3. Particle size distribution of a suspension of CeO₂ NPs with a nominal size of 1–10 nm. NP were spiked into (A) Milli-Q water or (B) rainwater. (C) Particle size distribution for Ce-containing NPs in rainwater, determined under the assumption that they were spherical CeO₂ NPs with a density of 7.13 kg dm⁻³ [23]. The dashed line corresponds to the SDL. The mean particle size ± polydispersity of the CeO₂ NPs was (A) 11.0 ± 5.8 nm; (B) 7.7 ± 2.4 nm and (C) 9.2 ± 6.1 nm. Measurements were obtained using the wet-SF-ICP-MS with a 50 μs dwell time.

2.3. Ce-Containing NPs in Natural Waters: Riverwater

When unspiked, unfiltered and undiluted St. Lawrence River water samples were analyzed by SP-ICP-MS for ¹⁴⁰Ce, the raw data clearly showed the presence of spikes, strongly indicating the presence of Ce containing NPs or, alternatively, larger particles with a minor Ce component (Figure S5). Under the assumption that the detected particles correspond to spherical CeO₂ NPs, particle size distributions could be estimated (Figure 4). An average particle size of 21.9 ± 0.8 nm was determined

for particles sampled from the Saint Lawrence River (means and errors correspond to triplicate samples) (Table 3). The larger particle size, as compared to the rainwater sample could be attributed to both analytical and geochemical differences, i.e., (i) the hardness ions in the St. Lawrence River ($\sim 130 \text{ mg L}^{-1}$) [24] are expected to induce some agglomeration of the NP; (ii) the lower pH of the rainwater (pH = 5.4), with respect to St. Lawrence River (pH = 6.8), could facilitate greater particle dissolution and (iii) the higher dissolved (background) Ce in the river water sample resulted in a higher SDL (6.2 nm, Table 3), which could slightly increase the overall average particle size. Note that $\sim 7\times$ more NPs and $\sim 60\times$ more particle mass was determined in the river water with respect to the rainwater. Ce NP concentrations in the river water were $107 \pm 26 \text{ ng L}^{-1}$ (Table 3), in line with concentrations predicted by modelling (24 ng L^{-1} , [25]; $0.6\text{--}100 \text{ ng L}^{-1}$, [26]) and the limited available experimental data ($0.4\text{--}5.2 \text{ ng L}^{-1}$, [27]). While it might be tempting to attribute the slightly higher concentrations of Ce NP to greater emissions in the St. Lawrence, it is more likely that additional NP were detected due to the lower detection limits in this study. Nonetheless, for the majority of detected NP, similar particle size distributions were determined in the St. Lawrence River (mean diameter $\sim 19 \text{ nm}$; Figure 4), as were observed in the Meuse and IJssel Rivers in the Netherlands ($14\text{--}21 \text{ nm}$, mean 19 nm) [27]. Such a narrow distribution of NP in such geographically different samples suggests either a similar source for the NP or similar removal processes such as agglomeration leading to removal of the larger particles [28,29].

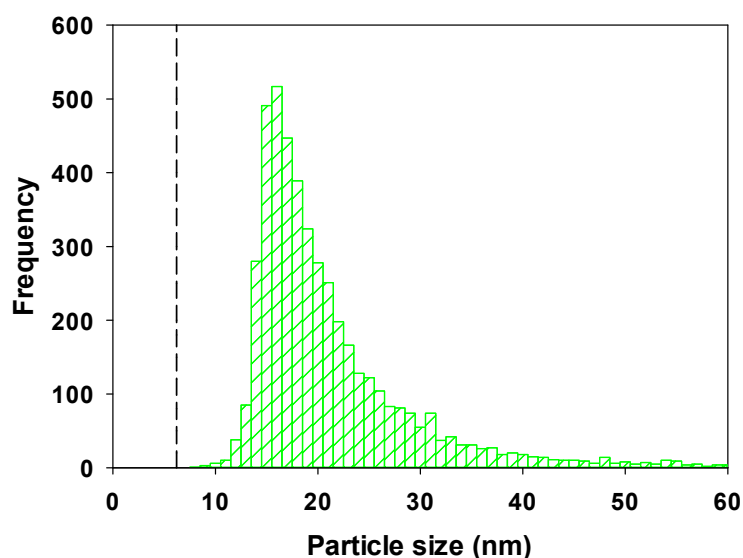


Figure 4. Particle size distributions of Ce containing NPs in a sample taken from the St. Lawrence River. The mean particle size \pm polydispersity corresponded to $21.0 \pm 9.2 \text{ nm}$. The dashed line corresponds to the SDL. Measurements were obtained using the wet-SF-ICP-MS with a $50 \mu\text{s}$ dwell time. NP sizes were calculated by assuming that the particles were spherical CeO_2 particles with a density of 7.13 kg dm^{-3} [23].

Table 3. Concentration of dissolved Ce, number and mass concentrations of CeO_2 NPs and SDL in the rainwater and in the St. Lawrence River. Means and standard deviations are obtained from the analysis of triplicate samples.

Water Natural Sample	Mass Concentration of Dissolved Ce (ng L^{-1})	Number Concentration ($\times 10^9 \text{ CeO}_2 \text{ NPs L}^{-1}$)	Mass Concentration of CeO_2 NPs (ng L^{-1})	SDL (nm)
Montreal rainwater	4.0 ± 0.1	0.22 ± 0.01	1.9 ± 0.1	4.6 ± 0.1
St. Lawrence River	53 ± 17	1.6 ± 0.3	107 ± 26	6.2 ± 0.6

2.4. Effect of Sample Filtration

Although the natural samples can be analyzed unfiltered, some of the larger particles can block the nebulizer. Given that we were interested in quantifying the smallest (nano) particles, the effect

of 0.45 μm membrane filtration was examined for a natural sample. For a St. Lawrence River water sample examined before or after filtration, filtration decreased background Ce concentrations by 30%, which was attributed to an adsorption of dissolved Ce on the filters. The decrease of dissolved Ce led to a decrease in the SDL, which may explain the small shift of the particle size distribution to lower sizes (Table S1 and Figure S6). Nonetheless, in spite of having a lower SDL, NP numbers decreased almost by 30% after filtration, which was attributed mainly to the removal of large particles (i.e., $>0.45 \mu\text{m}$) with some minor losses of Ce and/or small Ce-containing NPs to the filters via adsorption.

2.5. Ce-Containing NPs in Natural Waters: Temporal Variations

Temporal variations of the Ce NPs were examined by collecting rainwater samples between October 2018 and December 2018 and river water samples between August 2019 and September 2019. In the rainwater, the concentration of CeO_2 NPs varied from $(0.1\text{--}3.8) \times 10^8 \text{ L}^{-1}$, while they varied from $(1.1\text{--}7.2) \times 10^8 \text{ L}^{-1}$ in the river water (Figure 5A). Although particle number variations were more important in the rainwater (38 \times), as compared to the river water (7 \times), particle sizes were fairly similar in all samples (Figure 5B). In contrast, NP sizes in the river water were smaller than those detected previously in the same water catchment (St. Lawrence), but much further downstream stream (Figure 4). This result can be explained by the difference in sampling locations, which would indicate that the Ce-containing NPs are both time and geographically dependent (Figure S7).

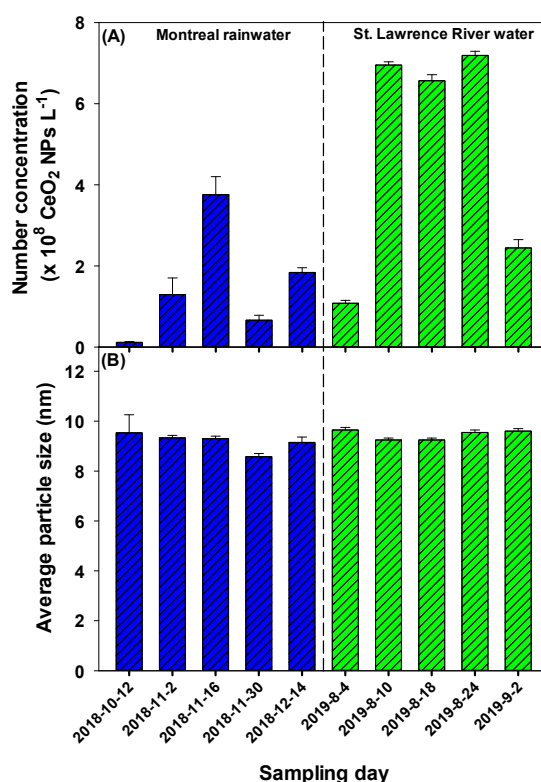


Figure 5. (A) Number concentrations and (B) mean particle sizes for CeO_2 NPs measured on different dates in rainwater (blue) and St. Lawrence River water (green). Error bars correspond to standard deviations obtained from triplicate analysis. Measurements were performed using wet-SF-ICP-MS and a dwell time of 50 μs .

2.6. Engineered or Natural CeO_2 NPs?

It is very difficult to non-ambiguously distinguish between engineered and natural NPs in the environment. Most commonly, it is assumed that engineered NPs (including metal oxides) contain a single metal, while natural NPs are often multi-element [30]. For Ce NP, the Ce/La ratio has been used

to differentiate the two types of NPs [31,32] since the rare earth elements are naturally nearly always found as mixtures. Natural NPs can be formed by mechanical erosion, weathering or precipitation [33] in which case, they are likely to have a similar composition as the minerals in sediments and soils. For example, Ce is found with La in minerals such as bastnasite with a Ce/La ratio of 1.5 [1,34] and in monazite with a Ce/La ratio of 1.8 [1,34]. In the earth's crust, a Ce/La ratio of 2.1 [35] has been documented. In that light, Montañó et al. [30] compared Ce/La ratios of nearly 100 surface water samples collected from three European countries to the Ce/La ratios of 807 water samples collected across a wide geographical range in Europe. In those samples, a fairly stable Ce/La ratio of 1.7 was measured.

In order to determine whether the NP contained only Ce or several metals, SF-ICP-MS was first used to measure individual particles for their Ce and La contents, albeit in different particles. Results were later validated with TOF-ICP-MS, run in single particle mode, which measures multiple elements in a single nanoparticle. The TOF-ICP-MS that was employed had a sensitivity for Ce ($597 \text{ counts fg}^{-1}$) that was about $8\times$ higher than the Q-ICP-MS ($72 \text{ counts fg}^{-1}$) but lower than the SF-ICP-MS ($14,800 \text{ counts fg}^{-1}$) and was necessarily limited to larger nanoparticles ($\text{SDL}\sim 11 \text{ nm}$).

The rainwater was analyzed for its Ce and La contents by SF-ICP-MS. Similar sensitivities were measured for La ($14,600 \pm 1700 \text{ counts fg}^{-1}$) and Ce ($13,600 \pm 500 \text{ counts fg}^{-1}$), which led to similar SDLs in the rainwater of $4.4 \pm 0.1 \text{ nm}$ for La_2O_3 and $4.6 \pm 0.1 \text{ nm}$ for CeO_2 . The raw data clearly indicated the presence of both Ce and La NPs or indeed composite NPs (Figure S8). As a control, no La (dissolved or NP) was detected in the suspension of 1–10 nm CeO_2 NPs. Detected Ce and La NPs showed similar mean sizes and size distributions (Table S2, Figure 6). Concentrations of both the dissolved and particulate forms of Ce were almost $2\times$ those of La with a Ce/La NP ratio of 2.2 ± 0.6 and a total Ce/La ratio of 2.4 ± 2.2 (Table 4). The slightly higher values, when compared to the expected global natural ratio of 1.7, was suggestive of the presence of engineered (single element) CeO_2 NPs in the rainwater.

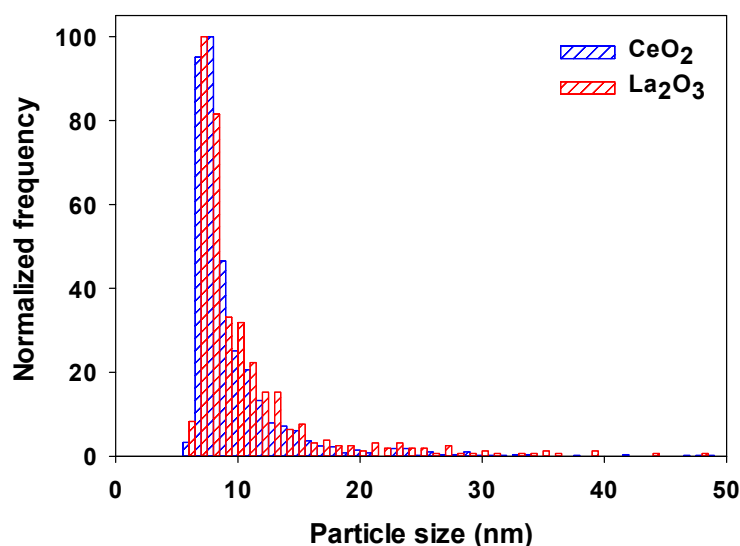


Figure 6. Particle size distributions of Ce- (blue) and La- (red) containing NPs found in a Montreal rainwater. Particle size distributions were calculated by assuming spherical particles of pure CeO_2 (density = 7.13 kg dm^{-3}) [23] and La_2O_3 (density = 6.51 kg dm^{-3}) [36]. Measurements were obtained using the wet-SF-ICP-MS with a $50 \mu\text{s}$ dwell time.

Table 4. Ratios of Ce to La determined in the Montreal rainwater, obtained using the SF-ICP-MS run in single particle mode with a dwell time of 50 μ s. Means and standard deviations were obtained from triplicate samples.

Water Natural Sample	Fraction of Ce NPs (%)	Fraction of La NPs (%)	Ce NPs/La NPs	Dissolved Ce/Dissolved La	Total Ce/Total La
Montreal rainwater	46.3 \pm 8.8	50.6 \pm 3.9	2.2 \pm 0.6	2.6 \pm 1.8	2.4 \pm 2.2

The rainwater sample was re-analyzed by TOF-ICP-MS in single particle mode. Given the size quantification limits (SQLs of \sim 16 nm for Ce and for La), only few Ce-containing particles were detected in the rainwater (1.5×10^6 L⁻¹). Nonetheless, for 36% of the Ce-containing nanoparticles in the rainwater, no second element was detected (Figure 7 and Figure S9).

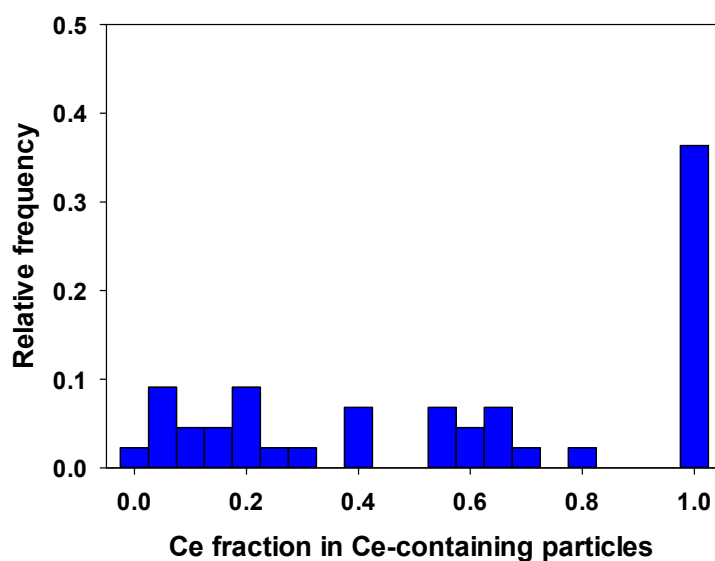


Figure 7. Detected proportion of Ce in Ce-containing particles measured in a Montreal rainwater. A Ce fraction of 1 indicates a pure Ce NP, while a fraction < 1 indicates the presence of other elements in the particles. Measurements were obtained using the TOF-ICP-MS with a 76.5 μ s dwell time; SDL (Ce) = 11 nm and SQL (Ce) = 16 nm.

3. Materials and Methods

3.1. Engineered NPs

The cerium oxide NPs used in this study were purchased as an aqueous dispersion of citrate stabilized CeO₂ NPs with a nominal size range of 1–10 nm (Nanobyk[®]-3810, Byk, Weiser, Germany). Silver and gold NPs were used to determine transport efficiency and validate instrumental sensitivity and precision. Ag NPs were purchased from NanoComposix (San Diego, CA, USA) as a citrate stabilized suspension with nominal sizes of either 10 nm (NanoXact, AGCN10) or 20 nm (NanoXact, AGCN20). Three Au NPs were used. One was purchased as citrate stabilized suspension from NanoComposix (10 nm, NanoXact, AUCN10), a second was a monodisperse poly(ethylene glycol) carboxylated Au NP (30 nm, UltraUniform, AUXU30, NanoComposix) and a third was acquired from the National Institute of Standards and Technology (60 nm, NIST, SRM 8013, Gaithersburg, MD, USA).

NP stock suspensions were stored in the dark at 4 °C until use. Prior to analysis, the stock suspensions were vortexed for one minute, sonicated for 10 min (Branson Ultrasonic Cleaner, 5510R-DTH Model, 135 W), diluted to adequate concentrations in Milli-Q water ($R > 18.2$ M Ω cm; total organic carbon < 1 μ g L⁻¹), and then re-vortexed for one minute. Final suspensions had a mass concentration between 10–50 ng L⁻¹, depending on the NP size. Concentrations were optimized in order to ensure a statistically significant number of events, while reducing the probability for the concurrent

atomization and ionization of more than one NP (which would lead to an overestimation of particle size and underestimation of particle number). To evaluate the impact of background noise on NP size and concentration determinations, a 10 ng L^{-1} suspension of the Nanobyk[®] CeO₂ NPs was spiked with $5\text{--}100 \text{ ng L}^{-1}$ of ionic Ce purchased from Inorganic Ventures (CGCE1, Christianburg, VA, USA).

The total Ce concentration was determined by adding $400 \mu\text{L}$ of HNO₃ (67–70%) and $300 \mu\text{L}$ of H₂O₂ (30%) to 1 mL of the sample, prior to heating the mixture at $80 \text{ }^\circ\text{C}$ for 5 h (DigiPREP, SCP science, Montreal, Canada). Samples were then diluted to 2% *v/v* HNO₃ prior to their analysis by ICP-MS, using the ionic Ce (CGCE1) for calibration and indium (CGIN1) as an internal standard. Ce and In standards were purchased from Inorganic Ventures.

3.2. Sampling and Sample Preparation

Rainwater samples were collected, between October and December 2018, using wide-mouth polypropylene containers (500 mL, Fisher Scientific), which were placed on the 7th floor roof of the Roger-Gaudry Pavillon of the University of Montreal (Montreal, QC, Canada). St. Lawrence River water samples were collected from two different locations (Figure S7), between August and September 2019, using polypropylene tubes (50 mL, Fisher Scientific), at a depth of 20–30 cm, 1 m from the shore. All samples were stored at $4 \text{ }^\circ\text{C}$ in the dark. Prior to their analysis, water samples were first shaken manually, sonicated for 10 min, vortexed for one minute and then filtered through a $0.45 \mu\text{m}$, 33 mm diameter PVDF syringe filter. Filters were pre-rinsed with Milli-Q water and 5 mL of sample.

3.3. Instrumentation

Single particle ICP-MS data was acquired in fast scan mode using a quadrupole ICP-MS (Q-ICP-MS; Perkin Elmer NexION 300X, Woodbridge, ON, Canada) or a double focusing magnetic sector field ICP-MS (SF-ICP-MS; Nu AttoM ES, Nu Instruments, Wrexham, UK). The introduction system for the Q-ICP-MS consisted of a quartz cyclonic spray chamber, a type C0.5 concentric glass nebulizer (0.5 mL min^{-1}) and a quartz 2 mm bore injector. In the case of the SF-ICP-MS, two introduction systems were used: (i) A micro-flow concentric glass nebulizer (self-aspiration rate of $200 \mu\text{L}/\text{min}$ for 1 L min^{-1} argon gas) with a quartz cyclonic spray chamber cooled to $4 \text{ }^\circ\text{C}$ (wet-SF-ICP-MS); or (ii) an Apex Omega desolvator (Elemental Scientific, Omaha, NE, USA). When using the desolvator (dry-SF-ICP-MS), the sample was nebulized, with a PFA (perfluoroalkoxy) concentric micro-flow nebulizer (self-aspiration rate of $200 \mu\text{L min}^{-1}$) in a quartz cyclonic spray chamber that was heated to $140 \text{ }^\circ\text{C}$ before condensation at $3 \text{ }^\circ\text{C}$ and passage through a porous PFA membrane heated at $160 \text{ }^\circ\text{C}$. Argon was used as the membrane sweep gas ($6\text{--}8 \text{ L min}^{-1}$) and as the nebulizer gas ($0.7\text{--}1.0 \text{ L min}^{-1}$). In both introduction systems, the aerosol was injected into the plasma through a 1.5 mm internal diameter quartz injector.

Time of flight ICP-MS (TOF-ICP-MS) measurements were performed on a time-of-flight ICP-MS (Vitesse, Nu Instruments, Wrexham, UK) that allowed for multi-element characterization of individual nanoparticles. The instrument used a segmented reaction cell in which $4\text{--}6 \text{ cm}^3 \text{ min}^{-1}$ of He and ca. $4 \text{ cm}^3 \text{ min}^{-1}$ of H₂ gas was introduced in order to eliminate argon and nitrogen-based interferences for elements such as Si, K, Ca, Cr and Fe [37]. Time of flight mass spectra (23–238 amu) were acquired with a dwell time of $76.5 \mu\text{s}$ [37]. Total sample acquisition time was 32 s. In some experiments, the instrument was coupled to an Aridus II desolvator (Teledyne Cetac Technologies, Omaha, NE, USA) (Argon was used as the membrane sweep gas ($5\text{--}6 \text{ L min}^{-1}$) and as the nebulizer gas ($0.9\text{--}1.0 \text{ L min}^{-1}$)). Calibrations were performed using different custom-prepared standards (CLMS-1, CLMS-2, CLMS-3 and CLMS-4, SPEX CertiPrep, Metuchen, NJ, USA) that included all of the metals and metalloids.

3.4. SP-ICP-MS Data Acquisition

Triplicate samples were each analyzed three times- means and standard deviations were determined from the triplicate samples and triplicate measurements. In addition, in some cases, the breadth of the particle size distributions was indicated by calculating polydispersities. The isotopes

^{107}Ag , ^{197}Au , ^{139}La and ^{140}Ce were measured using a resolution of 300 and a dwell time of 50 μs . Data were acquired for 50 s at a sample flow rate of 100–200 $\mu\text{L min}^{-1}$. External calibrations (0.05 to 1.0 $\mu\text{g L}^{-1}$) were performed using ionic standards (Ag, La and Ce: Inorganic Ventures; IV-ICP-MS-71A; Au: Inorganic Ventures; MSAU-100PPM, Christianburg, VA, USA). Sensitivities were validated with an ionic quality control standard provided by High-Purity Standards (QCS-27). Transport efficiency (TE) was determined [38] by measuring the instrument sensitivity for ionic Au standards and the particle number concentration of a standard suspension of Au NPs. For analysis with the Q-ICP-MS, a 50 ng L^{-1} suspension of 60 nm Au NPs (NIST) was used for TE determinations, while for SF- and TOF-ICP-MS, a suspension of ultra-uniform 30 nm Au NPs (NanoComposix) was prepared daily at 20 ng L^{-1} . Furthermore, TE was validated by verifying the sizes of Ag NPs (NanoComposix) with a nominal size of 20 nm. TE values for the Q-ICP-MS were between 3–5%. With SF-ICP-MS, they were between 4–7%, except when using the desolvator (15–20%). For the TOF-ICP-MS, TE values ranged between 10–15%.

3.5. SP-ICP-MS Data Processing

Q-ICP-MS data were processed using the Syngistix Nano Module (Perkin Elmer, Woodbridge, ON, Canada). Peaks were considered if their intensity was greater than the average background + three times the standard deviation of the background. SF-ICP-MS data were processed using Nu Quant software (version 2.2, Nu Instruments, Wrexham, UK [18,39]). A built-in algorithm searches in a fixed window (3–15 ms) for a peak maximum that is greater than the signal of the smoothed background. When a maximum is found, the algorithm searches for the pre- and post-inflection points, integrates the data between these points and subtracts local peak background. Local peak background is determined from smoothed data prior to the pre-inflection point of the peak. The script also calculates the full width half maximum (FWHM) for each peak, which was used on several occasions to identify artifacts and coincidence (overly large FWHM). A major difference between the programs is that the Syngistix module identifies peaks with respect to the average signal background, whereas Nu Quant employs the local background. In both cases, the concentration of dissolved metal is determined from the average background signal, obtained from the entire data set.

Size detection limits (nm) are determined from the threshold intensity (I_T) (counts) used to discriminate between NP and the background according to Equation (1) [15,18].

$$\text{SDL} = \left(\frac{6 \times 10^6 \times I_T}{\pi \times \rho \times S \times X} \right)^{\frac{1}{3}} \quad (1)$$

where ρ is the particle density (kg dm^{-3}), S is the sensitivity (counts fg^{-1}) and X is the fraction of measured element in the NP. Similarly, the size quantification limit (SQL) can be defined as the smallest diameters that can be detected with confidence. Thus, SDL is a mean value that is calculated from the sum of the threshold intensity (I_T) and 3 times its standard deviation (SD), whereas the SQL was determined from $I_T + 10\text{SD}$.

A modified version of NuQuant (Nu Instruments, UK) was used for the treatment of the TOF-ICP-MS data. In that case, the algorithm searched for a target isotope, i.e., ^{140}Ce , using similar smoothing and peak detection parameters as with SF-ICP-MS. Following detection of the Ce-containing peaks, each particle event was assigned start and end timestamps, which were used to integrate peaks for all other isotopes [37]. As above, the criteria to report peak events as NP were based on the FWHM values as well as the standard deviation of the background (for each isotope), which were used to estimate threshold values. Artifacts were flagged based upon abnormally large or small FWHM values. For the TOF-ICP-MS, thresholds were typically based upon 5–7 multiples of the standard deviation of the background, which were selected to remove most background artifacts, while optimizing the detection of the real NP peaks [37].

4. Conclusions

In conclusion, the use of a high sensitivity sector field ICP-MS with very short dwell times (50 μ s) improved sensitivity (200 \times more) and decreased SDL (4 \times less) for Ce, when compared to the use of a Q-ICP-MS. The sensitivity and SDL were further improved when the SF-ICP-MS was coupled to a desolvator; however, this setup was shown to be much more sensitive to the presence of the dissolved analyte. SF-ICP-MS was shown to be useful to detect and characterize Ce-containing NPs in natural samples such as rain or river water samples. The use of a TOF-SP-ICP-MS allowed us to show that around a third of the nanoparticles in the Montreal rainwater were engineered CeO₂ NPs.

Supplementary Materials: The following are available online, **Figure S1:** Time resolved signal of ¹⁴⁰Ce in a suspension of 10 ng L⁻¹ CeO₂ NPs spiked with 10 ng L⁻¹ of ionic Ce measured using different dwell times. **Figure S2.** Particle size distributions of a 10 ng L⁻¹ suspension of CeO₂ NPs with a nominal size range 1–10 nm spiked with ionic Ce. **Figure S3.** Time-resolved signal for ¹⁴⁰Ce in a 10 ng L⁻¹ suspension of CeO₂ NPs with a nominal size range 1–10 nm spiked with ionic Ce. **Figure S4.** Size detection limit as a function of concentration of dissolved Ce, as measured by wet-SF-ICP-MS and dry-SF-ICP-MS. **Figure S5.** Time-resolved signal for ¹⁴⁰Ce in (A) unfiltered rainwater and (B) unfiltered St. Lawrence River water. **Figure S6.** Particle size distributions of Ce containing NPs in St. Lawrence River water with or without filtration. **Table S1.** Mean particle sizes, NPs number concentrations, mass concentration of dissolved Ce and SDL for Ce containing NPs in St. Lawrence River water, with or without filtration. **Figure S7.** Sampling locations on the St. Lawrence River. **Figure S8.** Time-resolved signal for (A) ¹⁴⁰Ce and (B) ¹³⁹La in Montreal rainwater. **Table S2.** Mean particle sizes, NPs number concentrations and mass concentration of dissolved and nanoparticulate Ce and La in Montreal rainwater. **Figure S9.** Time-resolved signal for ¹³⁹La (red) and ¹⁴⁰Ce (blue) in Montreal rainwater analyzed by TOF-SP-ICPMS.

Author Contributions: A.A. and I.J. collected the samples and prepared them for single particle analysis. M.H. and I.J. processed the SF-ICP-MS data. A.A. conducted TOF-ICP-MS analysis and processed the data. K.J.W. supervised the study. I.J., M.H. and K.J.W. wrote the manuscript. All authors have read and agreed to the published version of the manuscript.

Funding: This research was funded by the Natural Sciences and Engineering Research Council of Canada (NSERC) and the Fonds de Recherche du Québec—Nature et technologies (FRQNT).

Acknowledgments: Phil Shaw (Nu Instruments) provided greatly appreciated technical assistance when using the prototype TOF ICPMS.

Conflicts of Interest: The authors declare that they have no conflict of interest.

References

1. Dahle, J.T.; Arai, Y. Environmental geochemistry of cerium: Applications and toxicology of cerium oxide nanoparticles. *Int. J. Environ. Res. Public Health* **2015**, *12*, 1253–1278. [[CrossRef](#)]
2. Sánchez-García, L.; Bolea, E.; Laborda, F.; Cubel, C.; Ferrer, P.; Gianolio, D.; da Silva, I.; Castillo, J. Size determination and quantification of engineered cerium oxide nanoparticles by flow field-flow fractionation coupled to inductively coupled plasma mass spectrometry. *J. Chromatogr. A* **2016**, *1438*, 205–215. [[CrossRef](#)] [[PubMed](#)]
3. Speed, D.; Westerhoff, P.; Sierra-Alvarez, R.; Draper, R.K.; Pantano, P.; Aravamudhan, S.; Chen, K.L.; Hristovski, K.; Herckes, P.; Bi, X.; et al. Physical, chemical, and in vitro toxicological characterization of nanoparticles in chemical mechanical planarization suspensions used in the semiconductor industry: Towards environmental health and safety assessments. *Environ. Sci. Nano* **2015**, *2*, 227–244. [[CrossRef](#)]
4. Sahu, T.; Bisht, S.S.; Das, K.; Kerkar, S. Nanoceria: Synthesis and biomedical applications. *Curr. Nanosci.* **2013**, *9*, 588–593. [[CrossRef](#)]
5. Cornelis, G.; Ryan, B.; McLaughlin, M.J.; Kirby, J.K.; Beak, D.; Chittleborough, D. Solubility and batch retention of CeO₂ nanoparticles in soils. *Environ. Sci. Technol.* **2011**, *45*, 2777–2782. [[CrossRef](#)]
6. Auffan, M.; Masion, A.; Labille, J.; Diot, M.-A.; Liu, W.; Olivi, L.; Proux, O.; Ziarelli, F.; Chaurand, P.; Geantet, C.; et al. Long-term aging of a CeO₂ based nanocomposite used for wood protection. *Environ. Pollut.* **2014**, *188*, 1–7. [[CrossRef](#)]
7. Dan, Y.; Ma, X.; Zhang, W.; Liu, K.; Stephan, C.; Shi, H. Single particle ICP-MS method development for the determination of plant uptake and accumulation of CeO₂ nanoparticles. *Anal. Bioanal. Chem.* **2016**, *408*, 5157–5167. [[CrossRef](#)]

8. Azimzada, A.; Farner, J.M.; Hadioui, M.; Liu-Kang, C.; Jreije, I.; Tufenkji, N.; Wilkinson, K.J. Release of TiO₂ nanoparticles from painted surfaces in cold climates: Characterization using a high sensitivity single-particle ICP-MS. *Environ. Sci. Nano* **2020**, *7*, 139–148. [[CrossRef](#)]
9. Clar, J.G.; Platten, W.E.; Baumann, E.J.; Remsen, A.; Harmon, S.M.; Bennett-Stamper, C.L.; Thomas, T.A.; Luxton, T.P. Dermal transfer and environmental release of CeO₂ nanoparticles used as UV inhibitors on outdoor surfaces: Implications for human and environmental health. *Sci. Total. Environ.* **2018**, *613–614*, 714–723. [[CrossRef](#)]
10. Scifo, L.; Chaurand, P.; Bossa, N.; Avellan, A.; Auffan, M.; Masion, A.; Angeletti, B.; Kieffer, I.; Labille, J.; Bottero, J.-Y.; et al. Non-linear release dynamics for a CeO₂ nanomaterial embedded in a protective wood stain, due to matrix photo-degradation. *Environ. Pollut.* **2018**, *241*, 182–193. [[CrossRef](#)]
11. Keller, A.A.; Lazareva, A. Predicted releases of engineered nanomaterials: From global to regional to local. *Environ. Sci. Technol. Lett.* **2014**, *1*, 65–70. [[CrossRef](#)]
12. Limbach, L.K.; Bereiter, R.; Müller, E.; Krebs, R.; Gälli, R.; Stark, W.J. Removal of oxide nanoparticles in a model wastewater treatment plant: Influence of agglomeration and surfactants on clearing efficiency. *Environ. Sci. Technol.* **2008**, *42*, 5828–5833. [[CrossRef](#)] [[PubMed](#)]
13. Tan, Z.; Yin, Y.-G.; Guo, X.-R.; Amde, M.; Moon, M.H.; Liu, J.; Jiang, G.-B. Tracking the transformation of nanoparticulate and ionic silver at environmentally relevant concentration levels by hollow fiber flow field-flow fractionation coupled to ICPMS. *Environ. Sci. Technol.* **2017**, *51*, 12369–12376. [[CrossRef](#)] [[PubMed](#)]
14. Proulx, K.; Hadioui, M.; Wilkinson, K.J. Separation, detection and characterization of nanomaterials in municipal wastewaters using hydrodynamic chromatography coupled to ICPMS and single particle ICPMS. *Anal. Bioanal. Chem.* **2016**, *408*, 5147–5155. [[CrossRef](#)] [[PubMed](#)]
15. Laborda, F.; Bolea, E.; Jiménez-Lamana, J. Single particle inductively coupled plasma mass spectrometry: A powerful tool for nanoanalysis. *Anal. Chem.* **2014**, *86*, 2270–2278. [[CrossRef](#)] [[PubMed](#)]
16. Birbaum, K.; Brogioli, R.; Schellenberg, M.; Martinoia, E.; Stark, W.J.; Günther, D.; Limbach, L.K. No evidence for cerium dioxide nanoparticle translocation in maize plants. *Environ. Sci. Technol.* **2010**, *44*, 8718–8723. [[CrossRef](#)]
17. Roh, J.-Y.; Park, Y.-K.; Park, K.; Choi, J. Ecotoxicological investigation of CeO₂ and TiO₂ nanoparticles on the soil nematode *Caenorhabditis elegans* using gene expression, growth, fertility, and survival as endpoints. *Environ. Toxicol. Pharmacol.* **2010**, *29*, 167–172. [[CrossRef](#)]
18. Hadioui, M.; Knapp, G.; Azimzada, A.; Jreije, I.; Frechette-Viens, L.; Wilkinson, K.J. Lowering the Size Detection Limits of Ag and TiO₂ Nanoparticles by Single Particle ICP-MS. *Anal. Chem.* **2019**, *91*, 13275–13284. [[CrossRef](#)]
19. Fréchette-Viens, L.; Hadioui, M.; Wilkinson, K.J. Quantification of ZnO nanoparticles and other Zn containing colloids in natural waters using a high sensitivity single particle ICP-MS. *Talanta* **2019**, *200*, 156–162. [[CrossRef](#)]
20. Hadioui, M.; Peyrot, C.; Wilkinson, K.J. Improvements to single particle ICPMS by the online coupling of ion exchange resins. *Anal. Chem.* **2014**, *86*, 4668–4674. [[CrossRef](#)]
21. Abad-Álvarez, I.; Peña-Vázquez, E.; Bolea, E.; Bermejo-Barrera, P.; Castillo, J.R.; Laborda, F. Evaluation of number concentration quantification by single-particle inductively coupled plasma mass spectrometry: Microsecond vs. millisecond dwell times. *Anal. Bioanal. Chem.* **2016**, *408*, 5089–5097. [[CrossRef](#)] [[PubMed](#)]
22. Donovan, A.R.; Adams, C.D.; Ma, Y.; Stephan, C.; Eichholz, T.; Shi, H. Detection of zinc oxide and cerium dioxide nanoparticles during drinking water treatment by rapid single particle ICP-MS methods. *Anal. Bioanal. Chem.* **2016**, *408*, 5137–5145. [[CrossRef](#)] [[PubMed](#)]
23. US Research Nanomaterials, I. Cerium Oxide Nanopowder/Nanoparticles. Available online: <https://www.us-nano.com/inc/sdetail/214> (accessed on 1 November 2019).
24. Thorp, J.; Lamberti, G.; Casper, A. *St. Lawrence River Basin*; Elsevier academic press: Burlington, MA, USA, 2005; pp. 982–1028.
25. O'Brien, N.; Cummins, E. Nano-scale pollutants: Fate in Irish surface and drinking water regulatory systems. *Hum. Ecol. Risk Assess. Int. J.* **2010**, *16*, 847–872. [[CrossRef](#)]
26. Gottschalk, F.; Sun, T.; Nowack, B. Environmental concentrations of engineered nanomaterials: Review of modeling and analytical studies. *Environ. Pollut.* **2013**, *181*, 287–300. [[CrossRef](#)]
27. Peters, R.J.B.; Van Bommel, G.; Milani, N.B.; Hertog, G.C.D.; Undas, A.K.; van der Lee, M.; Bouwmeester, H. Detection of nanoparticles in Dutch surface waters. *Sci. Total. Environ.* **2018**, *621*, 210–218. [[CrossRef](#)]
28. Oriekhova, O.; Stoll, S. Stability of uncoated and fulvic acids coated manufactured CeO₂ nanoparticles in various conditions: From ultrapure to natural Lake Geneva waters. *Sci. Total. Environ.* **2016**, *562*, 327–334. [[CrossRef](#)]

29. Ramirez, L.; Gentile, S.R.; Zimmermann, S.; Stoll, S. Behavior of TiO₂ and CeO₂ nanoparticles and polystyrene nanoplastics in bottled mineral, drinking and lake geneva waters. impact of water hardness and natural organic matter on nanoparticle surface properties and aggregation. *Water* **2019**, *11*, 721. [CrossRef]
30. Montaña, M.D.; Lowry, G.V.; von der Kammer, F.; Blue, J.; Ranville, J.F. Current status and future direction for examining engineered nanoparticles in natural systems. *Environ. Chem.* **2014**, *11*, 351–366. [CrossRef]
31. Praetorius, A.; Gundlach-Graham, A.; Goldberg, E.; Fabienke, W.; Navratilova, J.; Gondikas, A.; Kaegi, R.; Günther, D.; Hofmann, T.; von der Kammer, F. Single-particle multi-element fingerprinting (spMEF) using inductively-coupled plasma time-of-flight mass spectrometry (ICP-TOFMS) to identify engineered nanoparticles against the elevated natural background in soils. *Environ. Sci. Nano* **2017**, *4*, 307–314. [CrossRef]
32. Markus, A.; Krystek, P.; Tromp, P.; Parsons, J.; Roex, E.; de Voogt, P.; Laane, R. Determination of metal-based nanoparticles in the river Dommel in the Netherlands via ultrafiltration, HR-ICP-MS and SEM. *Sci. Total. Environ.* **2018**, *631–632*, 485–495. [CrossRef]
33. Sharma, V.K.; Filip, J.; Zboril, R.; Varma, R.S. Natural inorganic nanoparticles—Formation, fate, and toxicity in the environment. *Chem. Soc. Rev.* **2015**, *44*, 8410–8423. [CrossRef] [PubMed]
34. Vitalij, K.; Karl, A.P.; Gschneidner, J. *Rare-Earth Element*; Encyclopaedia Britannica, inc.: Chicago, IL, USA, 2019; Available online: <https://www.britannica.com/science/rare-earth-element> (accessed on 24 November 2020).
35. Castor, S.B. Rare Earth Elements. In *Industrial Minerals & Rocks*; Society for Mining, Metallurgy, and Exploration, Inc.: Littleton, CO, USA, 2006; pp. 769–792.
36. US Research Nanomaterials, I. Lanthanum Oxide Nanopowder/Nanoparticles. Available online: <https://www.us-nano.com/inc/sdetail/965> (accessed on 1 November 2019).
37. Azimzada, A.; Farner, J.M.; Jreije, I.; Hadioui, M.; Liu-Kang, C.; Tufenkji, N.; Shaw, P.; Wilkinson, K.J. Single- and multi-element quantification and characterization of TiO₂ nanoparticles released from outdoor stains and paints. *Front. Environ. Sci.* **2020**, *8*. [CrossRef]
38. Pace, H.E.; Rogers, N.J.; Jarolimek, C.; Coleman, V.A.; Higgins, C.P.; Ranville, J.F. Determining transport efficiency for the purpose of counting and sizing nanoparticles via single particle inductively coupled plasma mass spectrometry. *Anal. Chem.* **2011**, *83*, 9361–9369. [CrossRef] [PubMed]
39. Shaw, P.; Donard, A. Nano-particle analysis using dwell times between 10 μ s and 70 μ s with an upper counting limit of greater than 3×10^7 cps and a gold nanoparticle detection limit of less than 10 nm diameter. *J. Anal. At. Spectrom.* **2016**, *31*, 1234–1242. [CrossRef]

Sample Availability: Not available.

Publisher’s Note: MDPI stays neutral with regard to jurisdictional claims in published maps and institutional affiliations.



© 2020 by the authors. Licensee MDPI, Basel, Switzerland. This article is an open access article distributed under the terms and conditions of the Creative Commons Attribution (CC BY) license (<http://creativecommons.org/licenses/by/4.0/>).